

# Automatic Parameter Selection for Denoising Algorithms Using a No-Reference Measure of Image Content

Xiang Zhu, *Student Member, IEEE*, and Peyman Milanfar, *Fellow, IEEE*

**Abstract**—Across the field of inverse problems in image and video processing, nearly all algorithms have various parameters which need to be set in order to yield good results. In practice, usually the choice of such parameters is made empirically with trial and error if no “ground-truth” reference is available. Some analytical methods such as cross-validation and Stein’s unbiased risk estimate (SURE) have been successfully used to set such parameters. However, these methods tend to be strongly reliant on restrictive assumptions on the noise, and also computationally heavy. In this paper, we propose a no-reference metric  $Q$  which is based upon singular value decomposition of local image gradient matrix, and provides a quantitative measure of true image content (i.e., sharpness and contrast as manifested in visually salient geometric features such as edges,) in the presence of noise and other disturbances. This measure 1) is easy to compute, 2) reacts reasonably to both blur and random noise, and 3) works well even when the noise is not Gaussian. The proposed measure is used to automatically and effectively set the parameters of two leading image denoising algorithms. Ample simulated and real data experiments support our claims. Furthermore, tests using the TID2008 database show that this measure correlates well with subjective quality evaluations for both blur and noise distortions.

**Index Terms**—Denoising, no-reference metric, parameter optimization, sharpness, singular value decomposition.

## I. INTRODUCTION

HUMANS have a remarkable capacity to perceive the content of a scene even when the image is disturbed by noise, blur, and other factors. That is to say, we seem to be able to register *true image content*<sup>1</sup> even when the pixels are highly corrupted across the image. It is self-evident then that a computable,

Manuscript received June 18, 2009; revised March 25, 2010 and May 24, 2010; accepted May 25, 2010. Date of publication June 14, 2010; date of current version November 17, 2010. This work was supported in part by the U.S. Air Force Grant FA9550-07-1-0365. The associate editor coordinating the review of this manuscript and approving it for publication was Prof. James E. Fowler.

The authors are with the Department of Electrical Engineering, University of California, Santa Cruz, Santa Cruz, CA 95064 USA (e-mail: xzhu@soe.ucsc.edu; milanfar@ee.ucsc.edu).

Color versions of one or more of the figures in this paper are available online at <http://ieeexplore.ieee.org>.

Digital Object Identifier 10.1109/TIP.2010.2052820

<sup>1</sup>By *true image content* we refer simultaneously to sharpness and local contrast, as manifested by visually salient geometric structures such as edges etc., which convey information about the nature of the physical objects in the scene. In this context, high frequency content such as that introduced by noise, or low frequency content such as that produced by blur of various types are not considered *true image content*.

quantitative measure of image content would be highly desirable. In this paper, we are concerned with the development of a such a scalar measure ( $Q$ ) of true image content. This measure is properly correlated with the noise level, sharpness and intensity contrast (which indicates the “visibility” [1]) of the structured regions of an image. For any given image, the nominal value of  $Q$  reacts in a natural way to the presence of noise and blur. Namely, its value generally drops if the variance of noise rises, and/or if the image content becomes blurry. With the definition of  $Q$  in hand, we will illustrate that it can be used effectively to optimize the performance of some leading denoising algorithms.

First, let us briefly summarize the relevant existing literature in this area. Objective quality [2] and sharpness metrics [3], [4] have been developed recently and can generally be divided into three categories: full-reference, reduced-reference and no-reference. Full-reference metrics need a complete reference image, and what they calculate is basically the similarity between the target and reference images. Such measures of similarity include the classical mean-squared error (MSE) and the recently introduced structural similarity (SSIM) [2]. Reduced-reference metrics require the reference image to be partially available, which is usually in the form of a set of extracted features [2]. However, in most practical applications the reference image is unavailable. Therefore, in applications such as denoising, deblurring, super-resolution (SR), and many other image reconstruction algorithms [2], the (full-reference) quality metrics MSE or SSIM can not be directly used to optimize the parameters of algorithms.

Several (no-reference) approaches have been developed to address the parameter optimization problem. Generalized cross-validation (GCV) [5], [6] and the L-curve method [7], [8] have been widely used in choosing the regularization parameters for various restoration applications. More recently, methods based upon Stein’s unbiased risk estimate (SURE) were proposed for the denoising problem [9], [10], which provide a means for unbiased estimation of the MSE without requiring the reference image. Useful as they are, these methods are far from ideal. Namely, aside from their computational complexity, they address the parameter optimization problem without direct regard for the visual content of the reconstructed images. Instead, they compute or approximate quantities such as MSE (or the related cross-validation cost), which are not necessarily very good indicators of visual quality of the results. As a particular example, for instance, Ramani *et al.*’s Monte-Carlo SURE [10], which can be used for arbitrary denoising algorithms, is based upon

the idea of probing the denoising operator with additive noise and manipulating the response signal to estimate MSE. This approach is also only appropriate when the noise is assumed to be Gaussian, and generally requires an accurate estimation of the noise variance as well.

In image restoration, as is the case for any estimation problem generally, it can be observed that selecting parameters amounts to a tradeoff between bias and variance in the final estimate. A canonical example is the regularization parameter in MAP-based restoration algorithms [5], [8]. Generally, the larger the parameter is, the more smooth the image content becomes (small variance), while more useful detail and edges are flattened or blurred (larger bias). In other words, an ideal no-reference measure that is useful for the parameter optimization problem should take both noise and blur on the reconstructed image into account [11]. However, most sharpness metrics [3], [4], [12], [13] can hardly distinguish image quality decay against high frequency behavior due to noise. Take the approach in [12] for example, whose value drops when the image is increasingly more blurred. The value of this measure also rises if the variance of noise is increased [see Fig. 8(e)]. For the metrics based upon edge detection and edge width estimation [4], the performance stability can easily suffer in the presence of noise. Such problems are precisely what our proposed metric  $Q$  is intended to address.

On a related note, we mention that some no-reference image quality metrics have been developed to detect noise and blur simultaneously. One example is the metric based upon the image anisotropy [14] proposed by Gabarda and Cristóbal [15]. They calculate the Rényi entropy [16] pixel by pixel along different directions, and use the variance of the entropy to index visual quality. However, such metrics require uniform degradation across the whole image, and do not work well if the random noise or blur varies spatially, which is the case, for instance, in images denoised by spatially adaptive filters.

The rest of this paper is organized as follows. We develop the definition of the metric<sup>2</sup>  $Q$  in several well-motivated steps. In Section II, we first introduce a preliminary metric  $H$ , which is based upon the local gradients of the image, as an intermediate step in arriving at  $Q$ . This metric can quantify the amount of blur and random noise, but requires prior knowledge or estimation of noise variance. Next, Section III gives the definition of the proposed metric  $Q$  and its statistical properties. Metric  $Q$  serves as an extension of the metric  $H$ , but does not depend upon prior knowledge about the noise variance. Simulated and real data experiments focused on optimizing parameters for various denoising algorithms using the metric  $Q$  are shown in Section IV. Finally, we summarize, conclude, and discuss directions of future research in Section V. We note that additional results and code are available at our project website.<sup>3</sup>

## II. LOCAL GRADIENTS AND THE SHARPNESS METRIC $H$

The aim of this section is to introduce some basic concepts including the image gradient matrix, the gradient covariance

<sup>2</sup>The proposed quantity is not a *metric* in the mathematical sense, but for convenience, we use this term interchangeably with *measure* when referring to  $Q$ .

<sup>3</sup><http://www.soe.ucsc.edu/~xzhu/doc/metricq.html>.

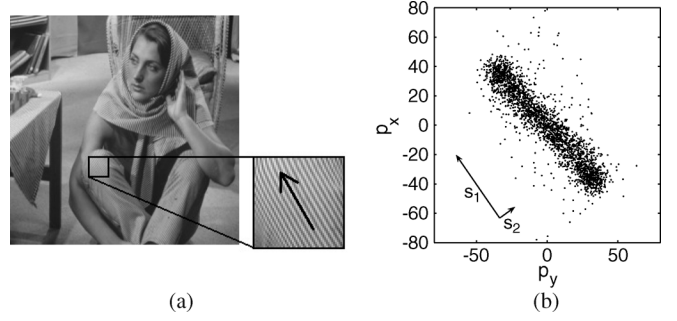


Fig. 1. Example of local dominant orientation estimation. (b) Plots the gradient of each pixel within the chosen patch in (a).  $s_1$  and  $s_2$  represent the energy in the dominant orientation and its perpendicular direction, respectively.

matrix, and their singular values and eigenvalues. Based upon these concepts and their performance in the presence of blur, a measure of sharpness which we term  $H$  is then proposed, which requires prior knowledge, or careful estimation, of noise variance across the whole image. As such, this measure is the basis of the main subject of this paper, which is the content measure  $Q$  that we subsequently define, analyze, and apply to the parameter selection problem.

It is well known that image structure can be measured effectively by using the differences in pixels (or image gradients). In particular, consider an image of interest  $p(x, y)$ . The gradient matrix over an  $N \times N$  window ( $w_i$ ) is defined as

$$\mathbf{G} = \begin{bmatrix} \vdots & \vdots \\ p_x(k) & p_y(k) \\ \vdots & \vdots \end{bmatrix}, \quad k \in w_i \quad (1)$$

where  $[p_x(k), p_y(k)]^T$  denotes the gradient<sup>4</sup> of the image at point  $(x_k, y_k)$ . The corresponding gradient covariance matrix is

$$\mathbf{C} = \mathbf{G}^T \mathbf{G} = \begin{bmatrix} \sum_{k \in w_i} p_x^2(k) & \sum_{k \in w_i} p_x(k)p_y(k) \\ \sum_{k \in w_i} p_x(k)p_y(k) & \sum_{k \in w_i} p_y^2(k) \end{bmatrix}. \quad (2)$$

Important information about the content of the image patch  $w_i$  can be derived from the gradient matrix  $\mathbf{G}$  or the gradient covariance matrix  $\mathbf{C}$ . In particular, we can calculate the local dominant orientation by computing the (compact) singular value decomposition (SVD) of  $\mathbf{G}$  [17] [18]

$$\mathbf{G} = \mathbf{U} \mathbf{S} \mathbf{V}^T = \mathbf{U} \begin{bmatrix} s_1 & 0 \\ 0 & s_2 \end{bmatrix} [\mathbf{v}_1 \quad \mathbf{v}_2]^T \quad (3)$$

where  $\mathbf{U}$  and  $\mathbf{V}$  are both orthonormal matrices. The column vector  $\mathbf{v}_1$  represents the dominant orientation of the local gradient field. Correspondingly, the second singular vector  $\mathbf{v}_2$  (which is orthogonal to  $\mathbf{v}_1$ ) will describe the dominant “edge orientation” of this patch. The singular values  $s_1 \geq s_2 \geq 0$  represent the energy in the directions  $\mathbf{v}_1$  and  $\mathbf{v}_2$ , respectively (see Fig. 1).

<sup>4</sup>The gradient can be estimated through the filters in (16) or (17) for instance.

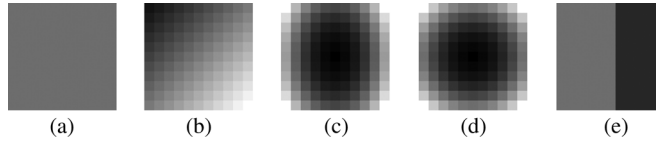


Fig. 2. Types of patches that are used in the experiments throughout this section. Gray levels are normalized to the range [0,1]. (a) Flat; (b) linear; (c) quadratic (anisotropic); (d) quadratic (isotropic); and (e) edged.

The previously shown quantities can equivalently be measured using the eigenvectors of  $\mathbf{C}$ , because

$$\mathbf{C} = \mathbf{V}\mathbf{S}^T\mathbf{S}\mathbf{V}^T = \mathbf{V} \begin{bmatrix} s_1^2 & 0 \\ 0 & s_2^2 \end{bmatrix} \mathbf{V}^T. \quad (4)$$

As we will describe in the following (and has been observed before [19]), since the singular values reflect the strength of the gradients along the dominant direction and its perpendicular direction, they are sensitive to blurring and, therefore, may be used to define a sharpness metric. But first, to gain some useful intuition, we analyze the behavior of  $s_1$  and  $s_2$  on several types of idealized patches which include flat, linear, quadratic, and edged regions (shown in Fig. 2).

In the flat case, all points within the  $N \times N$  patch share a common intensity value

$$p(x_k, y_k) = c. \quad (5)$$

Both  $p_x(k)$  and  $p_y(k)$  are equal to 0 for  $k = 1, 2, \dots, N^2$ , and  $s_1 = s_2 = 0$ . Naturally, ignoring boundary effects arising from the finite nature of the window, a flat patch remains unchanged after being blurred. In what follows, we will apply a space invariant Gaussian blur function with a growing spread to the canonical regions shown in Fig. 2, and observe how the singular values behave. In this sense, the flat region can be thought of as the asymptotic result as the spread of the blur function (or equivalently the strength of the blur) is made arbitrarily large.

In the linear patch, the gray value of each point can be modeled as

$$p(x_k, y_k) = a(x_k \cos \theta + y_k \sin \theta) + b \quad (6)$$

where  $a$  decides the slope,  $\theta$  decides the orientation, and  $b$  is the bias. It can be deduced that  $s_1$  and  $s_2$  have the following values:

$$\begin{aligned} s_1 &= aN \\ s_2 &= 0. \end{aligned} \quad (7)$$

Both  $s_1$  and  $s_2$  are independent from the orientation, and  $s_1$  is proportional to the slope given a fixed patch size, while  $s_2$  remains at zero.

The quadratic patch is modeled as

$$p(x_k, y_k) = a_1(x_k - x_c)^2 + a_2(y_k - y_c)^2 \quad (8)$$

where  $(x_c, y_c)$  is the center point. This kind of patch is called “isotropic” when  $a_1 = a_2$ , and “anisotropic” otherwise [see Fig. 2(c) and (d)]. The singular values of its gradient matrix are

$$\begin{aligned} s_1 &= a_{\max}N \sqrt{\frac{(N-1)(N+1)}{3}} \\ s_2 &= a_{\min}N \sqrt{\frac{(N-1)(N+1)}{3}} \end{aligned} \quad (9)$$

where

$$\begin{aligned} a_{\max} &= \max(a_1, a_2) \\ a_{\min} &= \min(a_1, a_2). \end{aligned} \quad (10)$$

Here  $s_1$  and  $s_2$  reflect the values of  $a_1$  and  $a_2$ , which determine the patch slope at each point and, thus, determine the sharpness and contrast of the region.

Another type of image region that is very sensitive to blurring is the ideal edged patch. In the interest of convenience we just look at an ideal vertical edge:

$$p(x_k, y_k) = \begin{cases} b+c, & x_n > x_c \\ b, & \text{otherwise} \end{cases} \quad (11)$$

where, without loss of generality,  $c$  is a positive constant. The corresponding singular values are

$$\begin{aligned} s_1 &= \frac{c}{2}\sqrt{2N} \\ s_2 &= 0. \end{aligned} \quad (12)$$

Only  $s_1$  here reflects the value of parameter  $c$ , which gives the intensity difference (contrast) between the two sides of the edge.

In general, and regardless of type, rotating a patch by an arbitrary angle  $\theta$  will not change the singular values of the gradient matrix. To see this, we note the relationship between the rotated gradient matrix  $\mathbf{G}_\theta$  and the unrotated  $\mathbf{G}$

$$\mathbf{G}_\theta = \mathbf{G}\mathbf{R}_\theta^T \quad (13)$$

where  $\mathbf{R}_\theta$  is the (orthonormal) rotation matrix

$$\mathbf{R}_\theta = \begin{bmatrix} \cos \theta & -\sin \theta \\ \sin \theta & \cos \theta \end{bmatrix}. \quad (14)$$

Therefore, the SVD of  $\mathbf{G}_\theta$  becomes

$$\mathbf{G}_\theta = \mathbf{U}\mathbf{S}(\mathbf{R}_\theta\mathbf{V})^T \quad (15)$$

which illustrates that the directions  $\mathbf{v}_1$  and  $\mathbf{v}_2$  are correspondingly rotated, but the singular values  $s_1$  and  $s_2$  remain unchanged.

It is observed through the previously shown analysis that the singular value  $s_1$  is quite intimately related with the sharpness and contrast of the local region. This is valid not only in regions with strong direction and contrast (edged patch (12)), but also in regions which may be isotropic (quadratic patch (9), (10), where  $a_1 = a_2$ ), or very smooth (linear patch (7)).

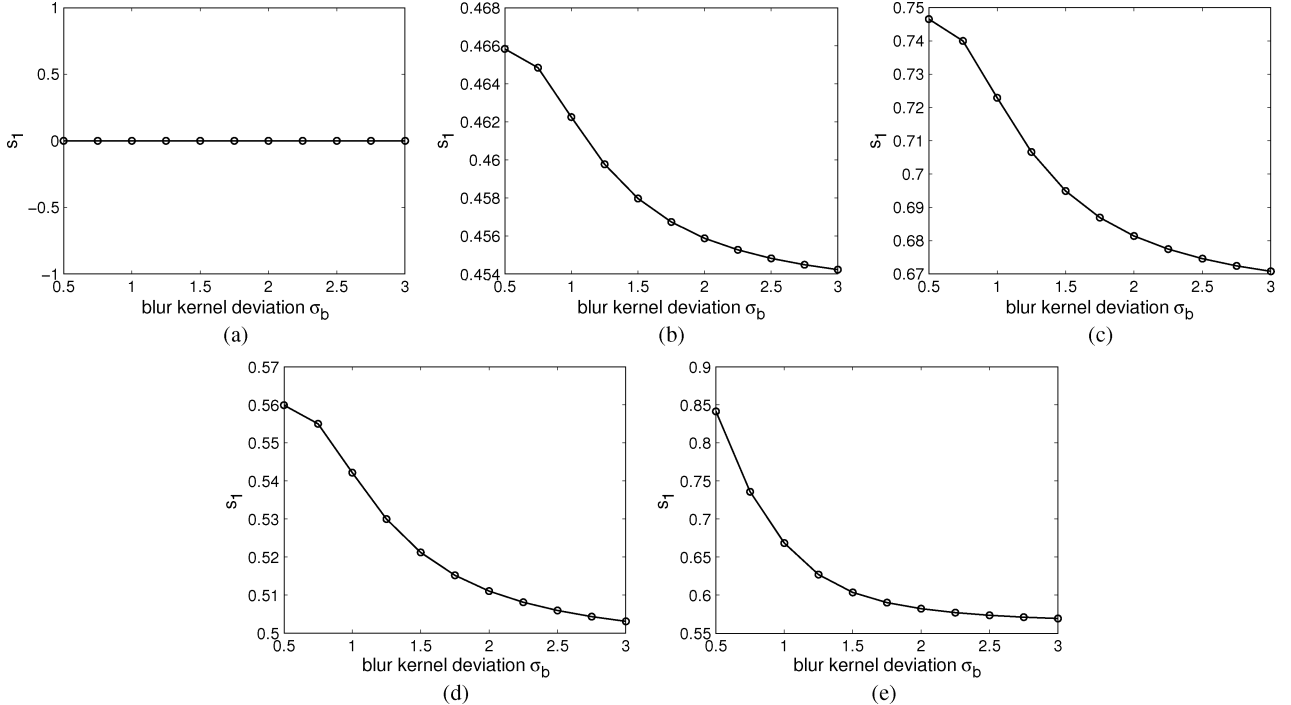


Fig. 3. Plots of  $s_1$  in blurring process for different patches. Patch size  $N = 7$ . The blur kernel is Gaussian, and the value of its standard deviation  $\sigma_b$  is raised steadily to make each patch more and more blurred. (a) Flat; (b) linear; (c) quadratic (anisotropic); (d) quadratic (isotropic); and (e) edged.

To verify the usefulness of  $s_1$  in the presence of blur, we applied a Gaussian blur kernel (of size  $5 \times 5$ ) with a steadily growing standard deviation  $\sigma_b$  to the previously mentioned patch types and recorded the resulting  $s_1$  values, which are shown in Fig. 3. The size of the patches is  $11 \times 11$ , and we only analyze the  $7 \times 7$  window in the center to avoid border effects. It is observed that as the value of  $\sigma_b$  grows (more blur),  $s_1$  for all the nonflat patches drops steadily as expected.

Next, we take noise into account. A good sharpness metric should react reasonably to both blur and random noise. So next we address what happens to  $s_1$  if the image (or patch) is corrupted by white (though not necessarily Gaussian) noise. Assume that we have an  $N \times N$  white noise image patch (with pixel-wise variance  $\sigma^2$ ) denoted in column-stacked vector format as an  $N^2 \times 1$  vector  $\mathbf{n}$ . In practice, the statistics of its gradient matrix  $\mathbf{G}_n$  depend upon the way we calculate the discrete derivatives. For example, the gradient of  $\mathbf{n}$  in  $x$  and  $y$  directions can be produced by applying the filters

$$\frac{1}{2} \times \begin{bmatrix} 0 & 0 & 0 \\ -1 & 0 & 1 \\ 0 & 0 & 0 \end{bmatrix}, \quad \frac{1}{2} \times \begin{bmatrix} 0 & -1 & 0 \\ 0 & 0 & 0 \\ 0 & 1 & 0 \end{bmatrix} \quad (16)$$

or the filters

$$\frac{1}{8} \times \begin{bmatrix} -1 & 0 & 1 \\ -2 & 0 & 2 \\ -1 & 0 & 1 \end{bmatrix}, \quad \frac{1}{8} \times \begin{bmatrix} -1 & -2 & -1 \\ 0 & 0 & 0 \\ 1 & 2 & 1 \end{bmatrix}. \quad (17)$$

The gradient matrix  $\mathbf{G}_n$  can be calculated as

$$\mathbf{G}_n = [\mathbf{D}_x \mathbf{n} \quad \mathbf{D}_y \mathbf{n}] \quad (18)$$

where the matrices  $\mathbf{D}_x$  and  $\mathbf{D}_y$  are derived from filters such as the ones just mentioned. Because the noise is zero-mean, the expected value of  $\mathbf{G}_n$  is

$$E(\mathbf{G}_n) = [0 \quad 0] \quad (19)$$

and the expected gradient covariance matrix becomes

$$\begin{aligned} E(\mathbf{C}_n) &= E(\mathbf{G}_n^T \mathbf{G}_n) \\ &= E\left(\begin{bmatrix} \mathbf{n}^T \mathbf{D}_x^T \mathbf{D}_x \mathbf{n} & \mathbf{n}^T \mathbf{D}_x^T \mathbf{D}_y \mathbf{n} \\ \mathbf{n}^T \mathbf{D}_y^T \mathbf{D}_x \mathbf{n} & \mathbf{n}^T \mathbf{D}_y^T \mathbf{D}_y \mathbf{n} \end{bmatrix}\right) \end{aligned} \quad (20)$$

where the first entry can be deduced as

$$\begin{aligned} E(\mathbf{C}_n)_{1,1} &= E(\mathbf{n}^T \mathbf{D}_x^T \mathbf{D}_x \mathbf{n}) \\ &= E(\text{tr}(\mathbf{D}_x \mathbf{n} \mathbf{n}^T \mathbf{D}_x^T)) \\ &= \sigma^2 \text{tr}(\mathbf{D}_x \mathbf{D}_x^T) \end{aligned} \quad (21)$$

and similarly we have

$$\begin{aligned} E(\mathbf{C}_n)_{1,2} &= \sigma^2 \text{tr}(\mathbf{D}_y \mathbf{D}_x^T), \quad E(\mathbf{C}_n)_{2,1} = \sigma^2 \text{tr}(\mathbf{D}_x \mathbf{D}_y^T) \\ E(\mathbf{C}_n)_{2,2} &= \sigma^2 \text{tr}(\mathbf{D}_y \mathbf{D}_y^T). \end{aligned}$$

The value of  $\text{tr}(\mathbf{D} \mathbf{D}^T)$  depends upon the specific filter used in (18). It can be shown that if we choose (16) or (17), the expected  $\mathbf{C}_n$  will have the form

$$E(\mathbf{C}_n) = \begin{bmatrix} \xi N^2 \sigma^2 & 0 \\ 0 & \xi N^2 \sigma^2 \end{bmatrix} \quad (22)$$

where  $\xi = 1/2$  if we use filters (16), and  $\xi = 3/16$  for filters in (17).

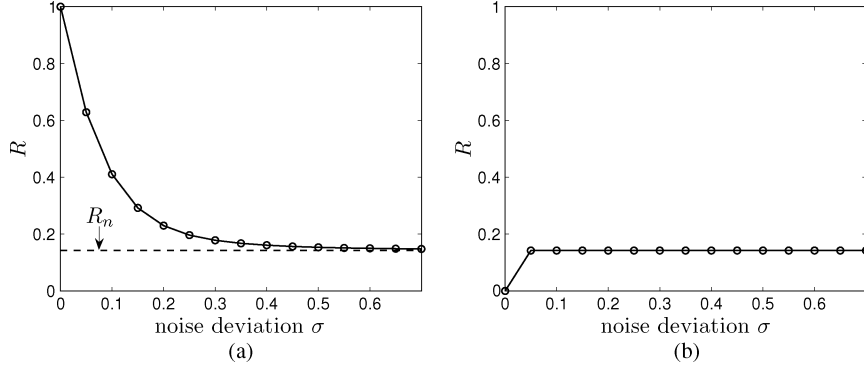


Fig. 4. Plots of the coherence  $R$  of a noisy edged patch (a) and a noisy flat patch (b) versus the noise standard deviation  $\sigma$ .  $R_n$  stands for the coherence of the noise sample.

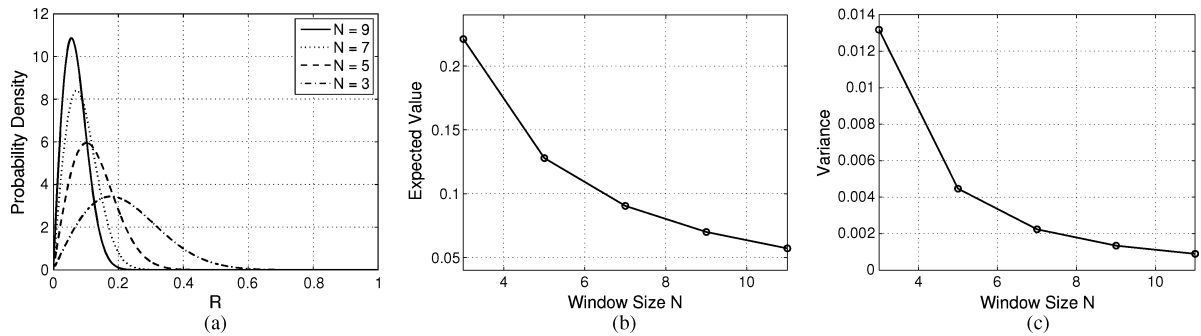


Fig. 5. Statistical properties of local coherence measure  $R$  for white Gaussian noise. (a) Probability density functions with different patch sizes. (b) Expected values. (c) Variances.

Now consider how the value of  $s_1$  changes when a clean image  $\mathbf{p}$  is corrupted by the white noise image denoted by  $\mathbf{n}$ . The gradient matrix of the noisy image  $\hat{\mathbf{p}}$  would become

$$\hat{\mathbf{G}} = \mathbf{G} + \mathbf{G}_n. \quad (23)$$

Since  $\mathbf{G}$  is deterministic, the expected  $\hat{\mathbf{C}}$  would have the form

$$\begin{aligned} E(\hat{\mathbf{C}}) &= E(\hat{\mathbf{G}}^T \hat{\mathbf{G}}) \\ &= \mathbf{G}^T \mathbf{G} + E(\mathbf{G}_n^T \mathbf{G}_n) + 2\mathbf{G}^T E(\mathbf{G}_n) \\ &= \mathbf{V} \begin{bmatrix} s_1^2 + \xi N^2 \sigma^2 & 0 \\ 0 & s_2^2 + \xi N^2 \sigma^2 \end{bmatrix} \mathbf{V}^T. \end{aligned} \quad (24)$$

So on average the dominant singular value  $\hat{s}_1$  of the noisy image can approximately be written as

$$\hat{s}_1 \approx \sqrt{s_1^2 + \xi N^2 \sigma^2}. \quad (25)$$

This equation tells us that  $\hat{s}_1$  is determined by both  $s_1$  and  $\sigma^2$ . Given a fixed  $\sigma^2$ , the value of  $\hat{s}_1$  drops as  $s_1$  is decreased, or say when the image  $\mathbf{p}$  becomes more blurry. Unfortunately,  $\hat{s}_1$  is also monotonically *increasing* with the noise variance  $\sigma^2$ .

To alleviate this problem, we define a modified metric  $H$  as follows:

$$H = \frac{\hat{s}_1}{\sigma^2}. \quad (26)$$

For now, we assume that the noise variance  $\sigma^2$  is known, or at least can be estimated. For a fixed  $\sigma^2$ , the behavior of  $H$  is basically the same as  $\hat{s}_1$ . If  $\sigma^2$  is sufficiently large,  $\hat{s}_1$  becomes approximately proportional to the standard deviation  $\sigma$

$$\hat{s}_1 \approx \xi^{1/2} N \sigma. \quad (27)$$

And, therefore, the value of  $H \approx (\xi^{1/2} N / \sigma)$  drops to zero with increasing  $\sigma$ , as desired. We note that in (26) the value of  $H$  estimated from patches in an image can be used to decide whether those patches contain real content (based upon sharpness and contrast) as opposed to noise. Said another way,  $H$  can be thought of as a rough indicator of the signal to noise ratio [19].

### III. IMAGE CONTENT METRIC $Q$

Although the metric  $H$  has well-behaved characteristics in the presence of both noise and blur,<sup>5</sup> it still suffers from the shortcoming that the variance of noise is assumed known or reliably estimated, which may not be the case in many real applications. As a practical example, if the image of interest is the output of a spatially adaptive denoising filter [20], it is difficult to estimate how much noise still remains, because the denoising effect varies with the local content in different parts of the image. So we need a metric which implicitly contains an estimate of the local noise variance as well. This is what we set out to do next.

<sup>5</sup>We refer interested readers to [19] for detailed experiments on  $H$ .

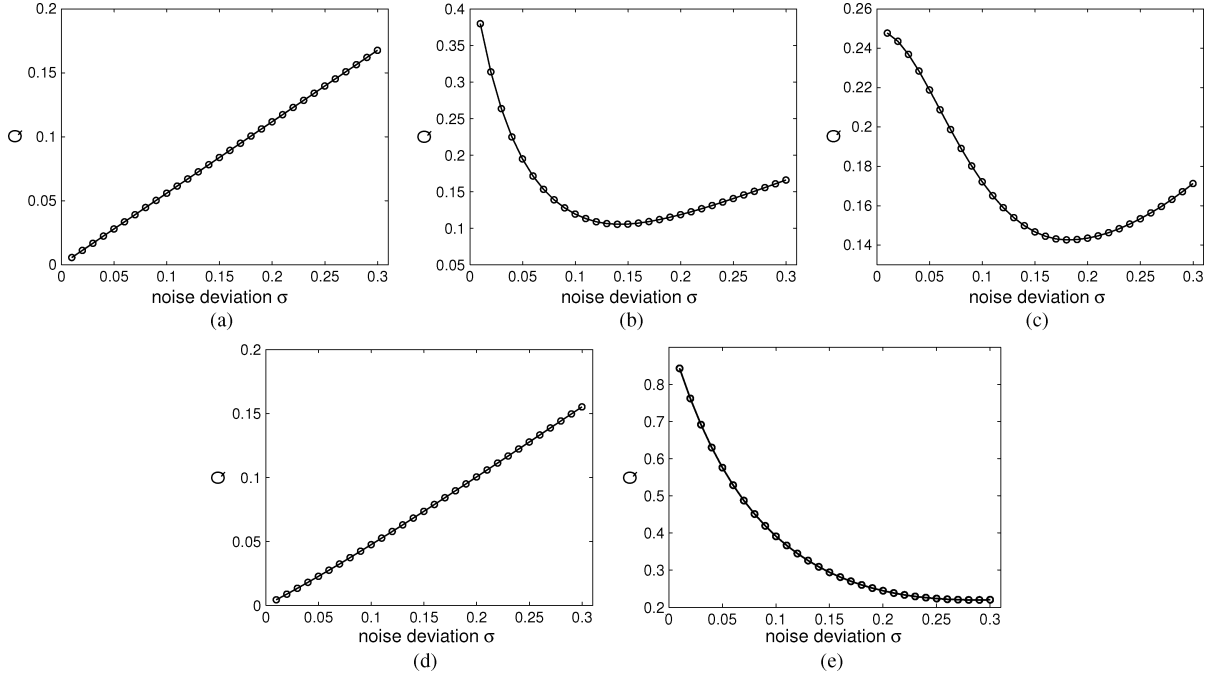


Fig. 6. Plots of the mean metric  $Q$  versus the noise standard deviation  $\sigma$  in Monte-Carlo simulations for different patches. 100 different noise realizations were used for each  $\sigma$  to get the averaged  $Q$ , and the patch size was  $N = 7$ . (a) Flat; (b) linear; (c) quadratic (anisotropic); (d) quadratic (isotropic); and (e) edged.

#### A. Definition of Metric $Q$ , Coherence $R$ and Their Statistical Properties

We define the image content metric  $Q$  as

$$Q = s_1 \frac{s_1 - s_2}{s_1 + s_2}. \quad (28)$$

Compared with  $H$  in (26), it can be seen that in the definition of  $Q$  the factor  $1/\sigma^2$  is replaced by another quantity, which we call the *coherence*

$$R = \frac{s_1 - s_2}{s_1 + s_2}. \quad (29)$$

As we briefly describe in the following, this replacement will not only do away with the explicit need to know the noise variance *a priori*, but also enables us to measure content even if the noise variance is nonstationary across the image.

Recall that for a noisy image patch  $\hat{\mathbf{p}}$ , its singular values  $\hat{s}_1$  and  $\hat{s}_2$  can approximately be written as:

$$\begin{aligned} \hat{s}_1 &\approx \sqrt{s_1^2 + \xi N^2 \sigma^2} \\ \hat{s}_2 &\approx \sqrt{s_2^2 + \xi N^2 \sigma^2} \end{aligned}$$

where  $s_1$  and  $s_2$  stand for singular values of a patch of the noise-free image  $\mathbf{p}$ . Replacing  $s_1$  and  $s_2$  by  $\hat{s}_1$  and  $\hat{s}_2$  in formula (29), we have

$$\begin{aligned} \hat{R} &\approx \frac{\sqrt{s_1^2 + \xi N^2 \sigma^2} - \sqrt{s_2^2 + \xi N^2 \sigma^2}}{\sqrt{s_1^2 + \xi N^2 \sigma^2} + \sqrt{s_2^2 + \xi N^2 \sigma^2}} \\ &= \frac{s_1^2 + \xi N^2 \sigma^2 - s_2^2 - \xi N^2 \sigma^2}{(\sqrt{s_1^2 + \xi N^2 \sigma^2} + \sqrt{s_2^2 + \xi N^2 \sigma^2})^2} \\ &= \frac{s_1^2 - s_2^2}{s_1^2 + s_2^2 + 2\xi N^2 \sigma^2 + 2\sqrt{(s_1^2 + \xi N^2 \sigma^2)(s_2^2 + \xi N^2 \sigma^2)}}. \end{aligned} \quad (30)$$

The previous equation illustrates that in a noisy image patch, the computed value of coherence  $R$  is roughly inversely proportional to the local noise variance  $\sigma^2$  when  $s_1 > s_2$  (which is true whenever the underlying patch is anisotropic.)

This is not the first time that coherence  $R$  has been used to analyze local image characteristics. Indeed, Bigun *et al.* [18] used this quantity to measure the locally dominant orientation of textures in a deterministic setting. In [17], we used this measure in a statistical framework to estimate dominant orientations in a multiscale setting. As mentioned before,  $s_1$  and  $s_2$  represent the energy in both the dominant direction and its perpendicular direction. So basically  $R$  measures their relative size. Considering a noise-free region with strong anisotropic geometric structure (such as the edged patch), the difference between  $s_1$  and  $s_2$  is very large, and in the absence of noise, the value of  $R$  is near 1. If white noise is added, the resulting  $R$  would be reduced, indicating that this region has become less structured, or the strength of the dominant direction has been reduced. It is worth repeating that metric  $Q$  is valid as an approximation of  $H$  only when the noise-free patch contains a dominant orientation (where  $s_1 > s_2$ ). The behavior of  $Q$  when the patch is isotropic (where  $s_1 = s_2$ ) will be discussed in the next subsection.

So far, the definition and descriptions of measures  $Q$  and  $R$  were quite general in the sense that the only assumption on noise was that it is white. It is instructive to study the statistical behavior of  $Q$  and  $R$  in a specific (Gaussian) noise setting. As may be expected, the statistical distribution of these metrics in the presence of noise of arbitrary distribution is in general very complex. However, their distributions are tractable when the noise is restricted to be white and Gaussian. For the sake of completeness, therefore, we next discuss the statistical behavior of  $R$  when the image patch is purely white Gaussian noise (WGN).<sup>6</sup>

<sup>6</sup>For the sake of completeness, the statistical distribution of  $Q$  is also given in the Appendix.

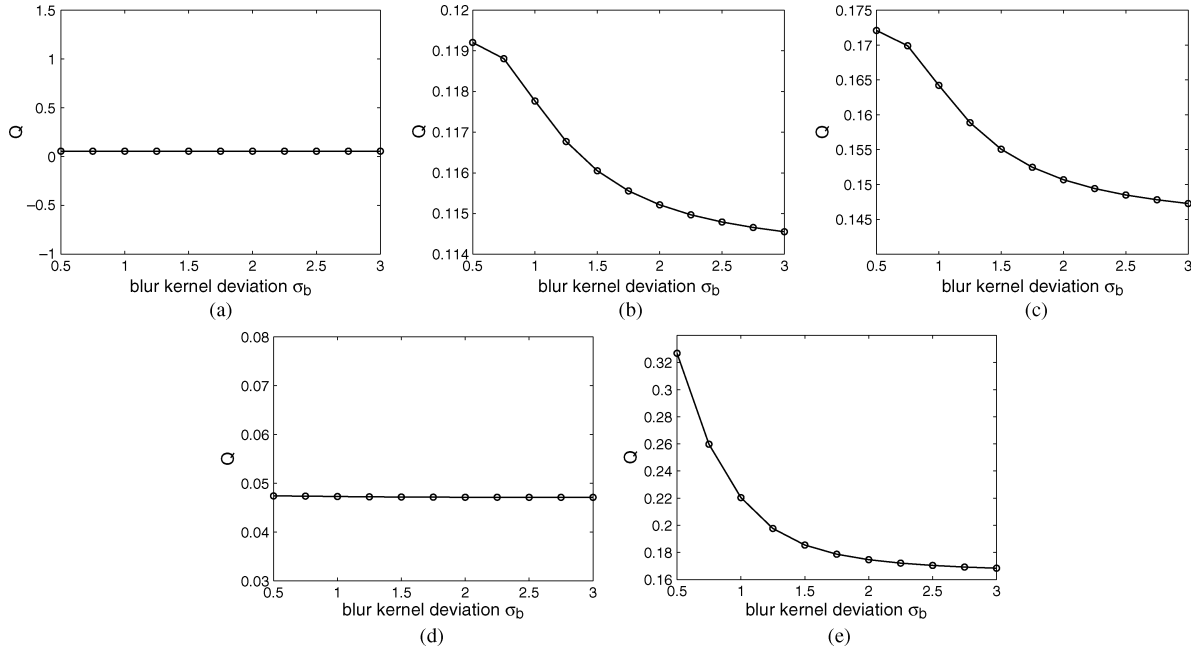


Fig. 7. Monte-Carlo simulations using both random noise and blur for different patches. Each patch was blurred first and then white Gaussian noise with  $\sigma = 0.1$  was added. After each blurring process, 100 independent noise simulations were applied, respectively, and averaged value of metric  $Q$  was calculated.  $N = 7$  and the size of the Gaussian smoothing kernel is  $5 \times 5$ . (a) Flat; (b) linear; (c) quadratic (anisotropic); (d) quadratic (isotropic); and (e) edged.

If the image patch  $\hat{\mathbf{p}}$  is pure WGN ( $s_1 \approx s_2 \approx 0$ ), according to (30) coherence  $R \approx 0$ , but in practice in a finite window size,  $R$  has a small positive value. Put another way, while in theory, a white noise images contains (by definition) no dominant orientation, patches with limited size lead to a small relative difference between  $\hat{s}_1$  and  $\hat{s}_2$ , leading to a nonzero coherence. More specifically, given a patch of white Gaussian noise pixels, the corresponding  $R$  is a random variable whose density function is (see Fig. 5 and Appendix for detailed derivation)

$$f_R(r) = 4(N^2 - 1)r \frac{(1 - r^2)^{N^2 - 2}}{(1 + r^2)^{N^2}}. \quad (31)$$

It is interesting to note that the pdf of  $R$  is independent of the mean and variance of the white noise; instead, it is a strong function of the patch size  $N^2$ .

We computed the coherence  $R$  on an edged patch (as described in (11), where  $b = 0.3$  and  $c = 0.5$ ) and a flat patch (as described in (5), where  $c = 0.5$ ) to illustrate its behavior in random noise. A sample of WGN  $\mathbf{n}$  is added to each patch with its standard deviation  $\sigma$  ranging from 0 to 0.7. The plots of the coherence  $R$  of each noisy edged patch are shown in Fig. 4(a). Since  $s_1 > s_2 = 0$  in the clean edged patch,  $R = 1$  when  $\sigma = 0$ . We can see that as  $\sigma$  increases, the value of  $R$  drops as desired, and approaches the value of  $R_n$ , which is the coherence of the noise-only sample  $\mathbf{n}$ . This is reasonable, because when  $\sigma \rightarrow \infty$ , the patch looks more and more like pure WGN. In the flat case [see Fig. 4(b)], where no anisotropic structure exists,  $R = R_n$  for all the nonzero noise standard deviations.<sup>7</sup> The random variable  $R_n$  is distributed according to the pdf (31).

The pdf of  $R$  for a variety of  $N$  is plotted in Fig. 5, where the change of the first and second moments of  $f_R(r)$  versus  $N$  are

<sup>7</sup>For the flat patch,  $s_1 = s_2 = 0$  when  $\sigma = 0$ . In such situations, we define  $R = 0$ .

also shown. We can see that the expected value of  $R$  decreases as  $N$  increases. This coincides with the fact that as the patch size grows, asymptotically there is no dominant direction in a noise patch. The reader may be wondering why we bother to derive and illustrate the statistical distribution of  $R$  as we have done here. This indeed turns out to be helpful in the latter part of this section, where the density function of  $R$  will be used in a significance test to tease apart isotropic patches from anisotropic ones. This distinction will then be employed in reliably calculating the metric  $Q$  for the whole image.

### B. Behavior of $Q$ in Different Patch Types

To further understand the performance of the image content metric  $Q$  in different types of patches in the presence of Gaussian noise, we employ Monte-Carlo simulations. White Gaussian noise with a variety of  $\sigma$ , ranging<sup>8</sup> from 0.01 to 0.3, was added to the test patches shown earlier. For each  $\sigma$ , 100 Monte-Carlo simulations are carried out with independent noise realizations. Fig. 6 shows the plots of the averaged  $Q$  across these experiments, versus the standard deviation of noise. In this experiment, we distinguish quadratic patches into isotropic ( $a_1 = a_2$ ) and anisotropic ( $a_1 \neq a_2$ ) types. It can be observed that the behavior of  $Q$  is consistent across all anisotropic patch types (including linear, anisotropic quadratic and edge), but different in the isotropic patches (including flat, and isotropic quadratic.)

It is no surprise to see that in isotropic cases,  $Q$  goes up steadily when  $\sigma$  rises, because the coherence part in  $Q$  cannot play the role of  $1/\sigma^2$  as we mentioned before. Take the flat patch for example. The coherence  $R$  does not change with the noise

<sup>8</sup>The pixel value is on a scale of [0, 1] gray level.

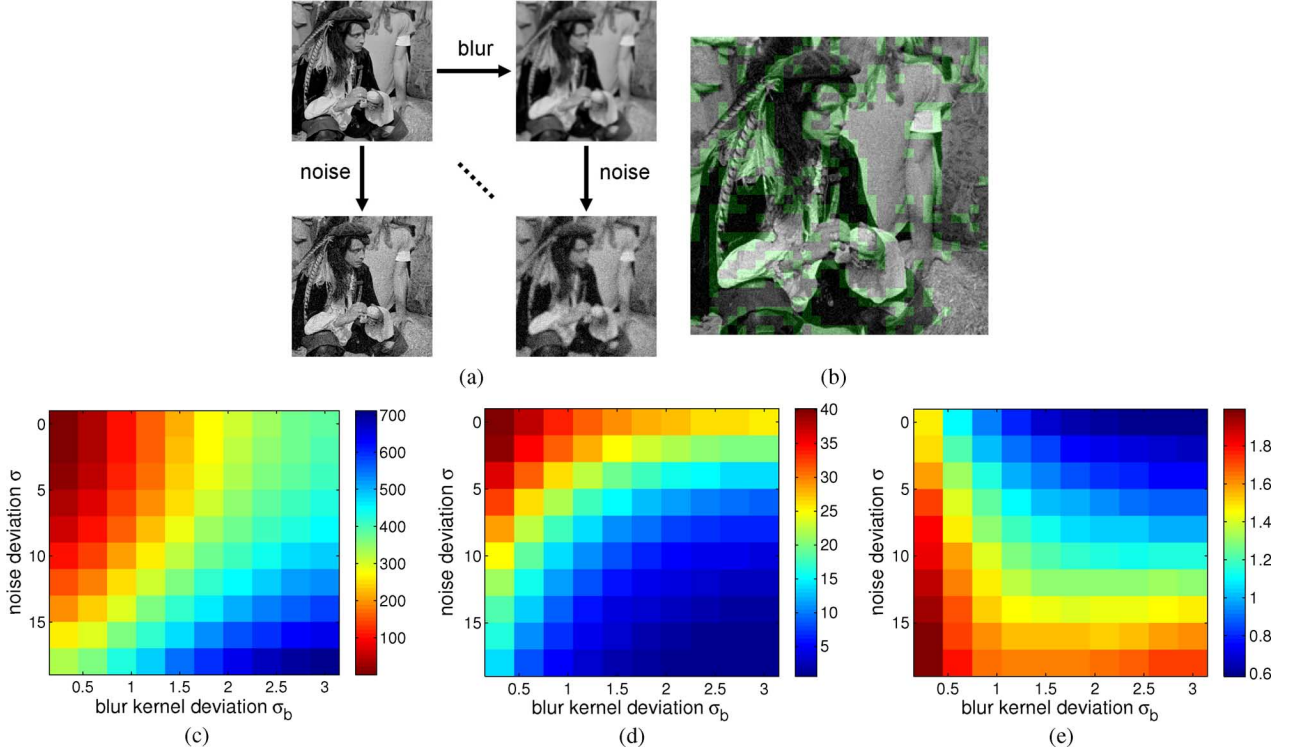


Fig. 8. Evaluations of  $Q$ , MSE and JNB [12] on the image **Man** ( $256 \times 256$ ), and its successively degraded versions. (a) Test image set; (b) anisotropic patches; (c) MSE; (d) metric  $Q$ ; (e) JNB. In (b), the green areas illustrate the anisotropic patch set used in measuring  $Q$ . In (c), we inverted the color scale just to show the similarity between MSE and  $Q$  in capturing the trend of image quality change.

variance [see Fig. 4(b)], while  $\hat{s}_1$  is proportional to  $\sigma$  [see (27)]. So in this case,  $Q$  also becomes proportional to  $\sigma$ .

For anisotropic cases,  $Q$  behaves reasonably, since the coherence part decreases as described in (30) with respect to the increase of the noise standard deviation  $\sigma$ . But when  $\sigma$  goes to infinity, the image patch looks more and more like pure noise. So the coherence part approaches the expected value of the random variable  $R$  characterized by the density function (31). This value is usually small, but not zero. While, on the other hand, the increase of the  $\hat{s}_1$  part in  $Q$  is approximately proportional to  $\sigma$ , hence, the value of  $Q$  rises again. Fortunately, this becomes a problem only when the noise standard deviation becomes extremely large.

Next, we take the blurring process into account. Blurred patches are obtained by applying a Gaussian smoothing filter with a growing standard deviation  $\sigma_b$ . After that, white Gaussian noise with variance  $\sigma^2$  is added, respectively. In Fig. 7, we can see that basically for all the anisotropic cases, the value of metric  $Q$  drops when the test region gets more and more blurred in the presence of noise as expected. While in isotropic cases,  $Q$  does not show significant change.

So what do we learn from the previously shown simulations? Namely, we can see that generally for anisotropic patches, where a dominant orientation exists, the proposed metric  $Q$  is able to detect both blur and random noise. So in practice, when measuring the true content of an image as a whole using  $Q$ , the anisotropic areas are detected and used to compute a global measure for the whole image. Put another way, isotropic patches should be avoided in the calculation of the overall image content metric  $Q$ . Specifically, one way to distinguish isotropic from anisotropic areas is by employing significance

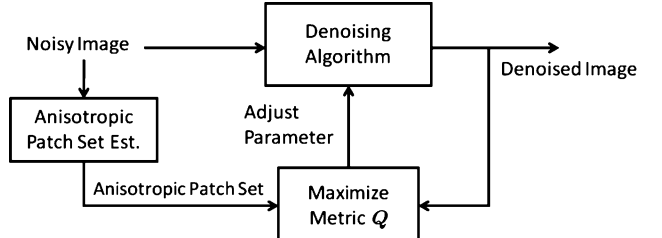


Fig. 9. Selecting the tuning parameter using metric  $Q$ .

testing based upon local coherence  $R$ , whose statistics in the “noise-only” case were described earlier in Section III-A.

Defining the null hypothesis  $\mathcal{H}_0$  as: “The given patch is isotropic with white Gaussian noise,” we can calculate the metric  $R$  and use it as a test statistics to decide whether to reject the null hypothesis  $\mathcal{H}_0$ . Numerically, the test is carried out by comparing the calculated  $R$  for the patch to a preselected threshold  $\tau$ . If  $R \geq \tau$ , then the hypothesis is rejected. For its part,  $\tau$  is determined by a significance level  $0 < \delta < 1$ , which is the probability of rejecting the null hypothesis when this hypothesis is in fact true. The relationship between  $\delta$  and  $\tau$ , which comes directly from integrating the pdf of  $R$ , is:<sup>9</sup>

$$\delta = \text{Prob}(R \geq \tau | \mathcal{H}_0) = \int_{\tau}^1 f_R(r) dr$$

<sup>9</sup>Strictly speaking, the density function used in the previous formula should be a valid pdf for  $R$  in all types of isotropic patches with WGN added; but this is not practical. Instead, for simplicity, we employ the pdf for pure WGN [see (31)] as an approximate and quite reasonable alternative.

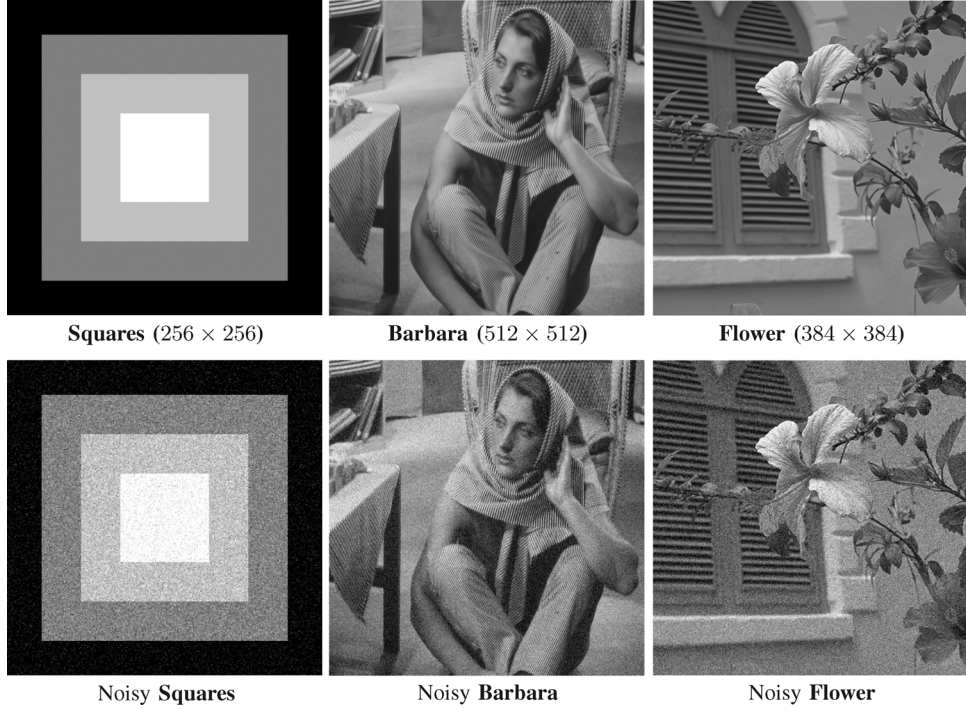


Fig. 10. Original images that are used in the simulated experiments, and the corresponding noisy images whose PSNR = 23 dB.

The integral of  $f_R(r)$  can be computed in closed form as

$$\delta = \int_{\tau}^1 f_R(r) dr = \left[ - \left( \frac{1-r^2}{1+r^2} \right)^{N^2-1} \right]_{\tau}^1 = \left( \frac{1-\tau^2}{1+\tau^2} \right)^{N^2-1}. \quad (32)$$

For a desired  $\delta$ , to determine the threshold, we can simply solve the previous equation for  $\tau$ . For example, if the patch size  $N = 8$ , and we want the significance level  $\delta$  to be 0.001, then the corresponding threshold becomes  $\tau = 0.2340$ . If the local coherence  $R \geq \tau$ , the test patch would be labeled as “anisotropic.”

### C. Detailed Algorithm for Computing $Q$

To summarize the previous discussions, we provide here a concise description of the algorithmic procedure for calculating the metric  $Q$  from a given image:

---

#### **Algorithm 1** Algorithmic Procedure for Computing $Q$

---

1. Given a noisy image, divide it into  $M$  nonoverlapping patches of size  $N \times N$ , and calculate the local coherence  $R_k$  using (29) for each patch  $k = 1, \dots, M$ .
  2. Find (say  $m \leq M$ ) anisotropic patches by thresholding the local coherence values as  $R_k \geq \tau$ . The threshold  $\tau$  is determined by solving the (32) with a given significance level  $\delta$ .
  3. Calculate the local metric  $Q_k$  using (28) on each anisotropic patch identified in step 2.
  4. Output the value  $Q = (1/M) \sum_{k=1}^m Q_k$  as the metric for the whole image.
- 

A simulated experiment using the natural image *Man* has been carried out to illustrate this procedure. The data in the test image set are generated through the following model:

$$\hat{\mathbf{p}} = \mathbf{p} \otimes \mathbf{k} + \mathbf{n} \quad (33)$$

where  $\mathbf{p}$  stands for the clean image,  $\mathbf{k}$  represents the blurring kernel,  $\otimes$  denotes the convolution, and  $\mathbf{n}$  is WGN.

We arranged the simulated images into a grid as shown in Fig. 8(a), where images get more and more blurred from left to right (by applying a  $9 \times 9$  Gaussian blur kernel with growing standard deviation  $\sigma_b$ ), and more and more noisy from top to bottom. The corresponding metric  $Q$ s (with the patch size  $N = 8$  and  $\delta = 0.001$ ) are given in Fig. 8(d). Full-reference metric MSE and a no reference sharpness metric JNB [12] are also tested for comparison. It can be observed that, like MSE, the change of the metric  $Q$  successfully reflects the change of the image quality, while the sharpness metric JNB (whose value drops as image becomes blurry,) failed in distinguishing quality decay against noise.

In the next section, we show how to apply  $Q$  to optimal parameter selection for some leading denoising algorithms.

### IV. USING $Q$ TO OPTIMIZE DENOISING ALGORITHMS

In this section, we will provide evidence that the proposed metric  $Q$  can be used to optimize the parameters of denoising algorithms. In particular, like [10], the application of  $Q$  to any “black-box” denoising algorithm with parameters in need of tuning is possible. We focus on two recent state of the art denoising algorithms.

One is the steering kernel regression (SKR) method of Takeda *et al.* [20], where there are two main parameters to tune: the global smoothing parameter  $h$ , and the iteration number. The

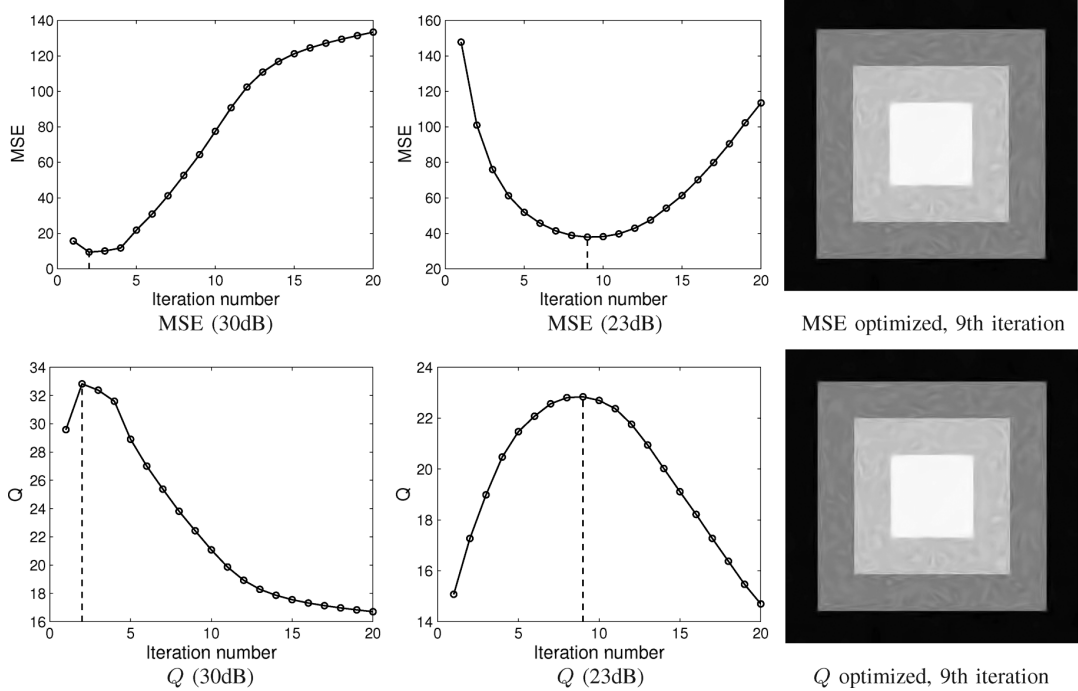


Fig. 11. Plots of MSE and metric  $Q$  versus iteration number in **SKR** denoising experiments using image **Squares**, and optimized filtered images (23 dB input).

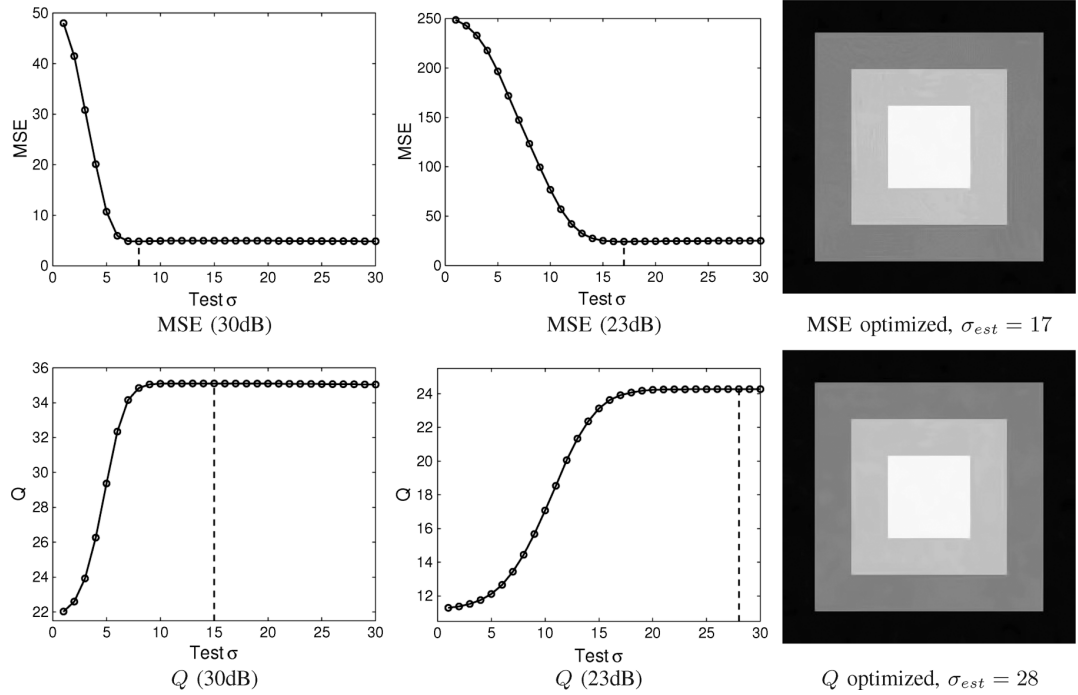


Fig. 12. Plots of MSE and metric  $Q$  versus the tuning parameter in **BM3D** denoising using image **Squares**, and optimized filtered images (23 dB input).

effect of these parameters is generally interdependent in that the smaller the  $h$  is, the more iterations are needed to achieve the best output image [20]. Hence, in practice, it makes sense to set  $h$  to a fixed value (we set it to 2.0 throughout) and to attempt to optimize the iteration number within a reasonable range (which we select to be between 1 and 20.)

The second algorithm is the block-matching and 3-D filtering (BM3D) algorithm [21], which is considered to be the state of the art denoising algorithm at the time of this writing. In the

BM3D filter, a Wiener filter is employed for collaborative filtering, which requires the estimate of a (variance) parameter  $\sigma_{est}^2$ . The value of the parameter  $\sigma_{est}$  can strongly affect the output and, thus, needs to be tuned. In the following experiments, we optimize this parameter in the broad range of 1 to 30.

In what follows, both simulated and real data are considered. In the simulated experiments, where the reference image is available (but not used in our case), MSE is also computed for

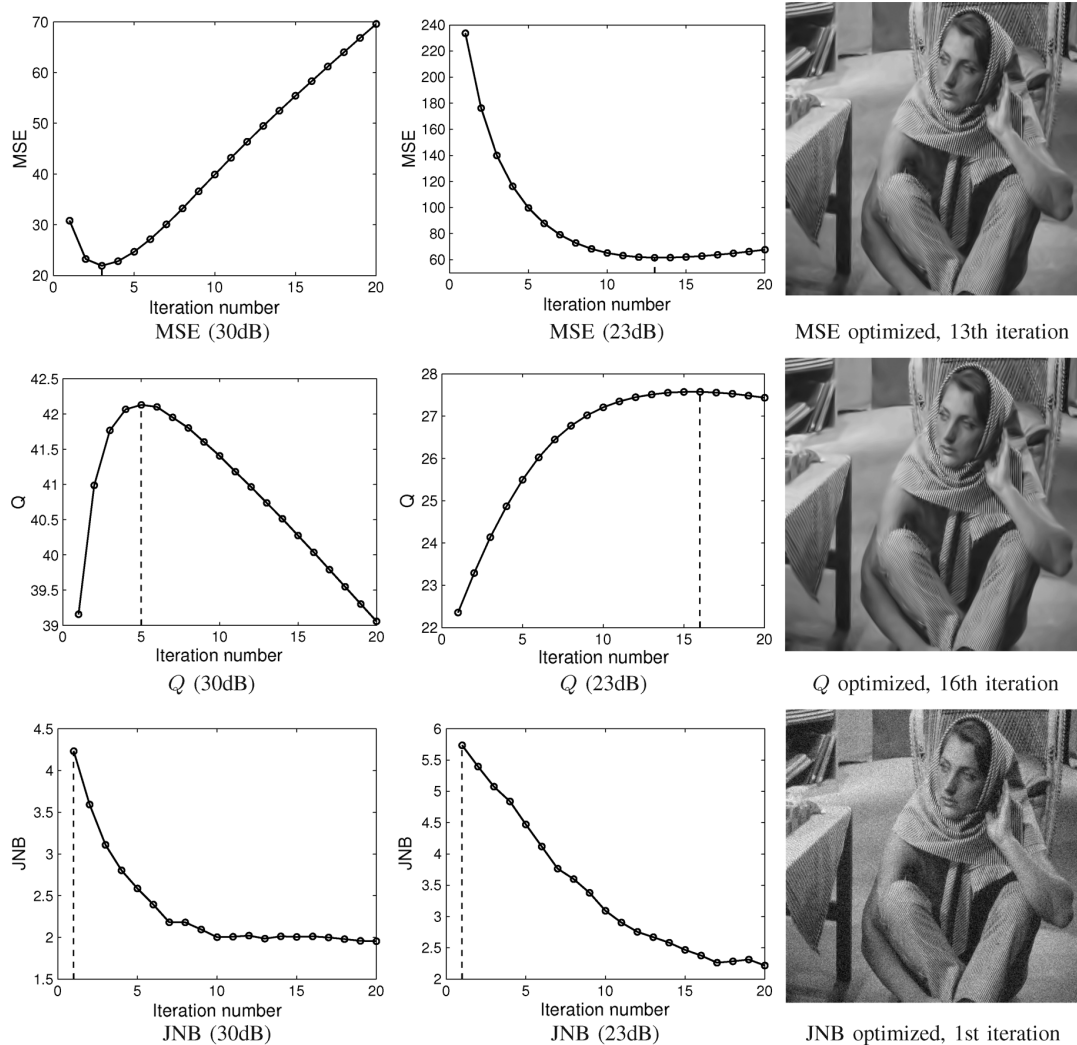


Fig. 13. Plots of MSE, metric  $Q$  and JNB [12] versus iteration number in **SKR** denoising experiments using image **Barbara**, and optimized filtered images (23 dB input).

the sake of comparison even though this calculation is not practical, and MSE is not a good visual metric anyway. Monte-Carlo SURE [10], on the other hand, offers a way to access MSE without a reference, and it is used for our experiments with a real noisy image.

In order to obtain a practical procedure for parameter setting, the strategy we take for computing the proposed metric  $Q$  is slightly different from what we described in Section III-C. Namely, we use the original noisy *input* image to estimate an anisotropic patch set  $\mathbf{m}$ , and use this reference set to compute the metric  $Q$  on the *output* of the respective denoising filter. We vary the value of the tuning parameter while observing the resulting  $Q$ . The “best” value of the algorithm parameter is then selected as that which maximizes the metric  $Q$  on the output (see Fig. 9). In all the following experiments for parameter optimization, we fix the patch size  $N = 8$ , and the significance level  $\delta = 0.001$  (or the threshold  $\tau = 0.2340$ ). From a practical point of view, insofar as computing  $Q$  is concerned, these values are universally good and do not need to be varied across images or in different context (or else this would defeat the very purpose of automatic parameter selection!) So we can compute

the metric  $Q$  with the same patch size and significance level in all the various experiments shown in this section. All the experiments are carried out on a desktop PC with Intel Pentium D CPU (3.00 GHz) in MATLAB. Computing  $Q$  for a  $512 \times 512$  output image takes around 0.25 s.

#### A. Simulated Experiments

In this set of experiments, we simulated noisy data by adding white Gaussian noise to three clean images shown in Fig. 10; namely, *Squares* ( $256 \times 256$ ), *Barbara* ( $512 \times 512$ ) and *Flower* ( $384 \times 384$ ). Experiments are conducted at peak signal-to-noise ratios<sup>10</sup> (PSNR) of 30 dB, and 23 dB, to test the performance of the metric in a range of noise strengths.

Plots of the experimental results are given in Figs. 11–16. We can observe that the metric  $Q$  was consistently effective in capturing the changing trend of quality in the output as the (SKR and BM3D) algorithm parameters were varied. As a result, the maximum value of  $Q$  yielded a very good result in every case

<sup>10</sup>Peak signal-to-noise ratio is defined as  $10 \log_{10}(255^2 / \sigma^2)$ , where  $\sigma^2$  is the variance of noise.

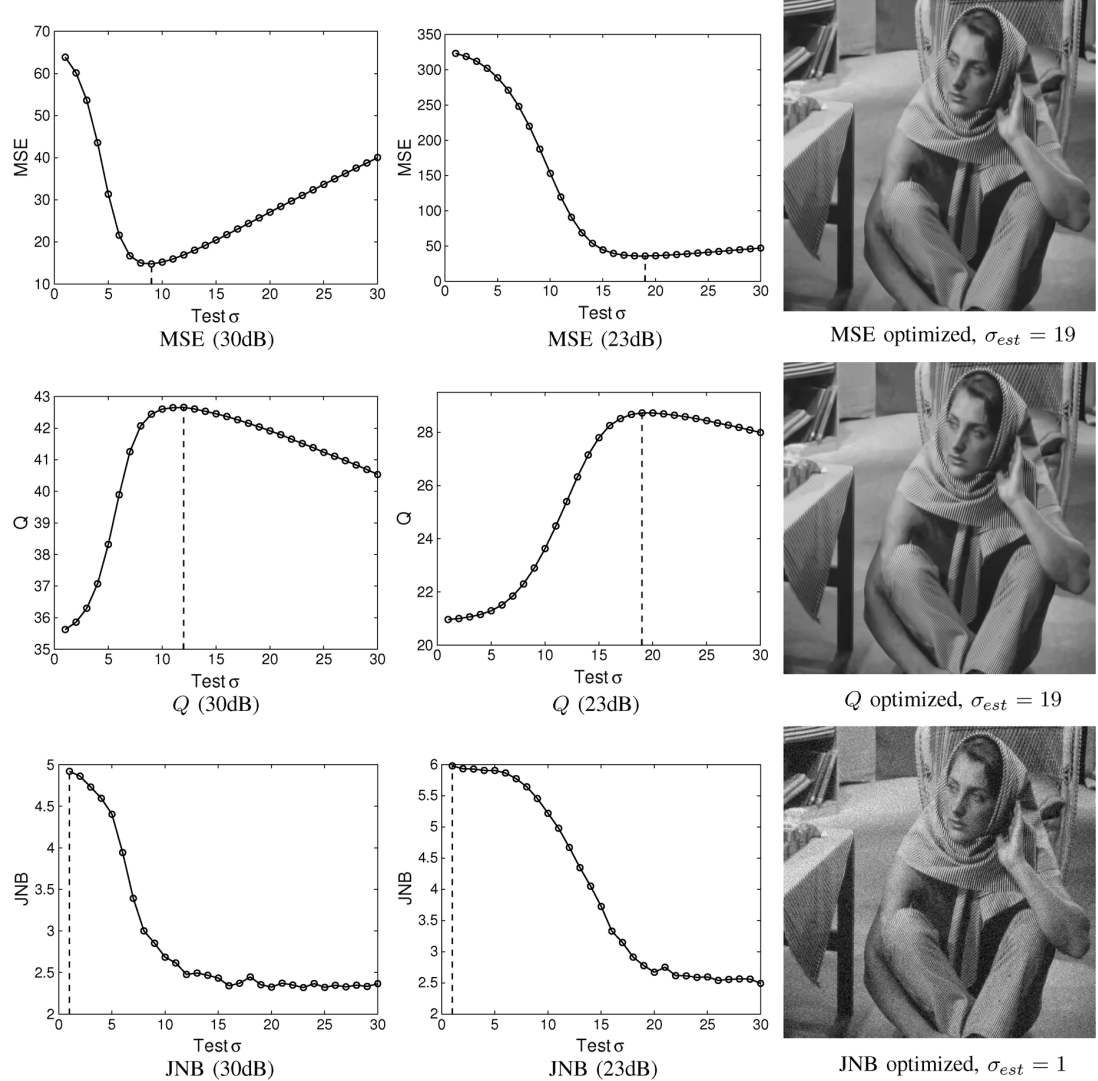


Fig. 14. Plots of MSE, metric  $Q$  and JNB [12] versus the tuning parameter in **BM3D** denoising experiments using image **Barbara**, and optimized filtered images (23 dB input).

in a completely unsupervised fashion and without access to a reference image or an estimate of the MSE. The behavior of  $Q$  provides not only an optimized value for the algorithm parameters, but also tends to reveal interesting behavioral characteristics of the algorithms to which it is applied. As a case in point, we observe that as the value of the parameter being optimized (number of iterations for SKR, and  $\sigma_{est}$  for BM3D) increases, the overall visual quality of the output image rises first due to the suppression of random noise, and then goes down because of the blurring effect of the filter. This phenomenon happens most strongly in the experiments using two natural images (*Barbara* and *Flower*)—see Figs. 13–16. In the *Squares* case, where the image content is relatively simple, the edges are successfully preserved by the BM3D filter even when the  $\sigma_{est}$  is set to be very large. This feature is also seen in the curves of both MSE and  $Q$  (see Fig. 12), where we can see the curves flattening out as the image quality changes little. The SKR algorithm, on the other hand, is more sensitive to increasing number of iterations, even when the content is relatively simple as in the *Squares* case, as can be seen in Fig. 11. For the sake of completeness, we also tried the no-reference sharpness metric JNB [12] to test its be-

havior and found that in general it fails to capture the trend of quality change since it cannot handle noise well. Examples are provided in Figs. 13 and 14.

### B. Real Noise Experiments

Fig. 17 illustrates a test image *JFK* ( $367 \times 343$ ) that suffers from real noise. The noise comes from film grain, scanning and compression processes, and is not Gaussian—indeed its variance is space varying. For lack of a better yardstick, we use the Monte-Carlo SURE [10] method for comparison, where the standard deviation of the noise (assumed to be globally constant) is estimated through the median absolute deviation (MAD) method [22]. The measured values for the previous test image is  $\sigma = 4.2$ . In implementing the Monte-Carlo SURE, the standard deviation of the probing noise is set to be 0.1 as recommended in [10].

Again, SKR and BM3D filters are employed in this set of experiments. The plots of SURE and  $Q$  versus the tuning parameter for the BM3D algorithm, and the corresponding optimized output images are provided in Fig. 19. For the SKR algorithm, plots of SURE and  $Q$  versus the iteration number and the cor-

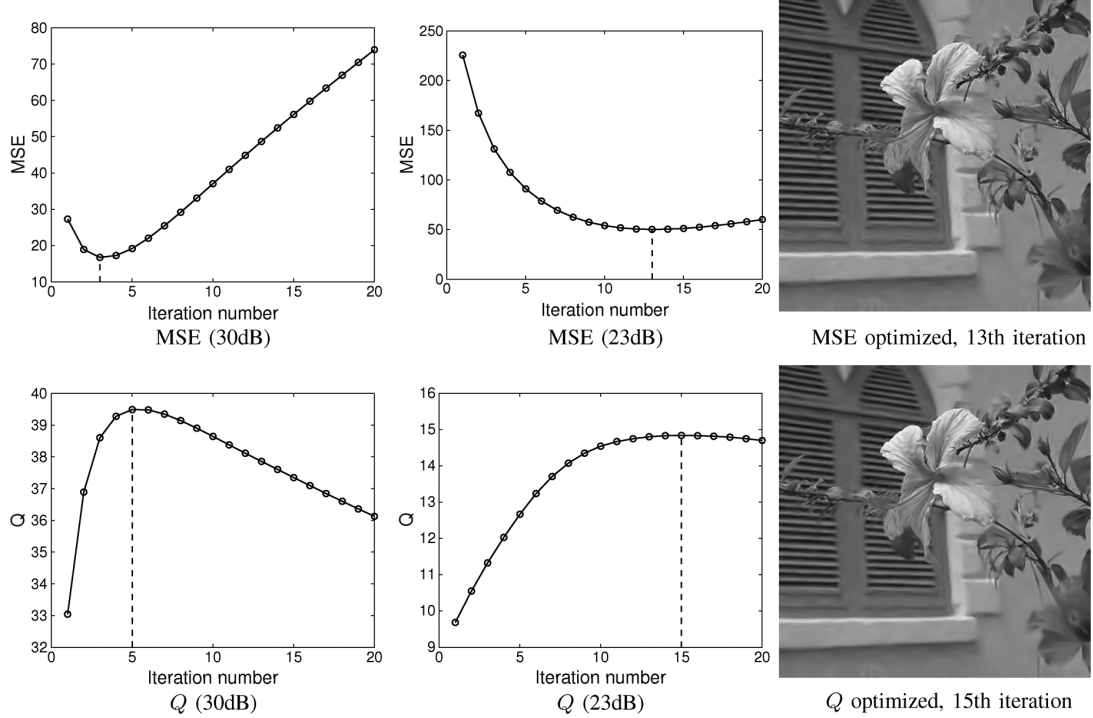


Fig. 15. Plots of MSE and metric  $Q$  versus iteration number in **SKR** denoising experiments using image **Flower**, and optimized filtered images (23 dB input).

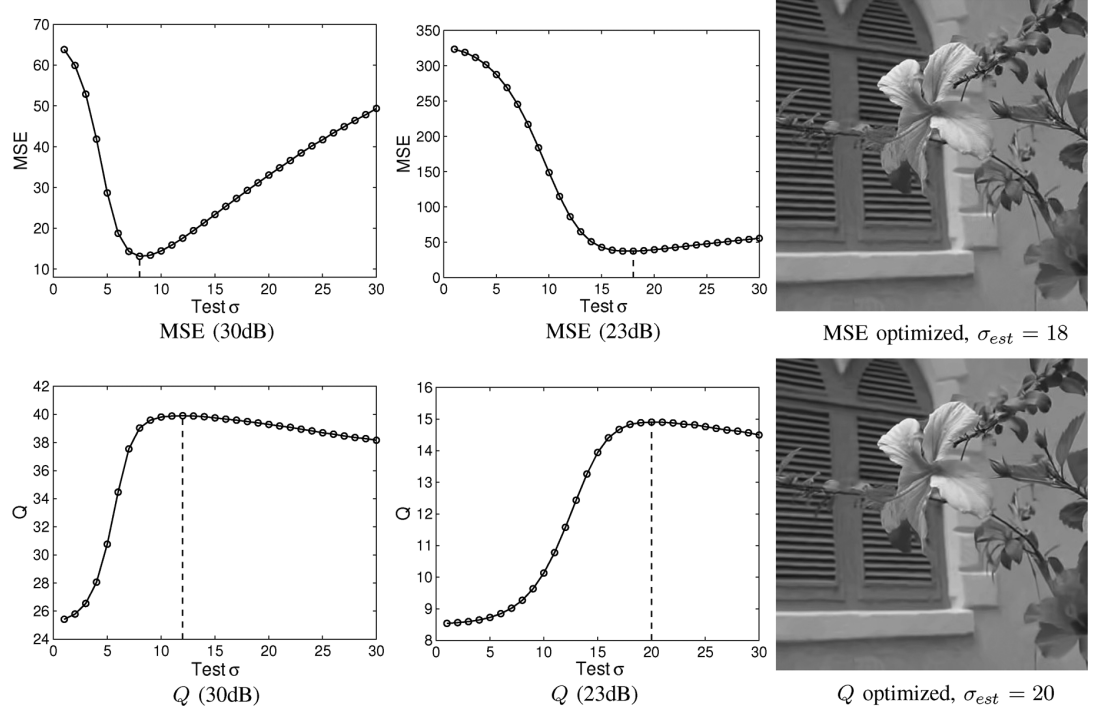


Fig. 16. Plots of MSE and metric  $Q$  versus the tuning parameter in **BM3D** denoising experiments using image **Flower**, and optimized filtered images (23 dB input).

responding optimized output images are provided in Fig. 18. For the SKR method, the optimal iteration number suggested by SURE is 1, which is clearly inadequate for denoising, as obvious noise can be observed in the output image. Meanwhile, the  $Q$  optimized iteration number shows good visual performance in balancing between denoising and detail-preservation. A similar phenomenon can be observed in the BM3D test (Fig. 19).

We note that since the noise is not white Gaussian, and the estimate of its standard deviation is likely inaccurate, this can lead to problems in the SURE calculation.

Through the previously shown real noise data experiments, it can be seen that the SURE method did not give adequate parameters for the filters when testing on the image *JFK*. This example is not entirely fair to the SURE method since the assumptions



Fig. 17. Image corrupted by real noise.

underlying that method are violated in this example. However, the experiment does illustrate that the metric  $Q$  is nevertheless able to maintain its stable performance, indicating that our proposed metric can be useful for a more general variety of practical situations.

### C. Correlation With Subjective Quality Scores

Finally we provide some tests based upon the TID2008 database [23] to illustrate the correlation between subjective ratings and the proposed no-reference parameter tuning system using metric  $Q$ . TID2008 database contains 25 reference images [some are illustrated in Fig. 20(a)–(c)] and each reference image  $\mathbf{p}_i$  ( $i = 1, 2, \dots, 25$ ) is degraded by several types of distortions (Gaussian blur, Gaussian noise, quantization noise, JPEG compression, etc.), where each type has four distortion levels. For each distorted version  $\hat{\mathbf{p}}_{ij}$  ( $j = 1, 2, \dots$ ), the corresponding mean opinion score (MOS) is also recorded and included in the database. In this section, we consider both Gaussian noise and Gaussian blur distortions as these are related to our application of interest. So for a given reference  $\mathbf{p}_i$ , we consider a set of corresponding degraded images  $\varphi_i = \{\hat{\mathbf{p}}_{ij} | j = 1, 2, \dots, 8\}$  including four noisy and four blurry images.

As illustrated in Fig. 9, in the parameter tuning system all the output images share the same anisotropic patch set  $\mathbf{m}$ , which is detected from the degraded input image, to compute the  $Q$ s. To faithfully illustrate the behavior of the proposed tuning system using  $Q$ , for every  $\hat{\mathbf{p}}_{ij} \in \varphi_i$  we also use the same anisotropic patch set  $\mathbf{m}_i$  to compute  $Q(\hat{\mathbf{p}}_{ij})$ , where  $\mathbf{m}_i$  is detected from the most noisy version within the set. We consider this image as an input, and other blurry or less noisy images the outputs from a denoising filter.

All 25 image sets from the database were tested. For each set  $\varphi$ , Spearman rank-order correlation coefficient (SROCC) [24] is employed to measure the correlation between MOS and the target metrics, including  $Q$ , MSE and JNB [12]. The average SROCC scores and the standard deviations are given in Table I (where test results using blurry image sets and noisy image sets separately are also provided). It can be observed that the performance of the proposed metric is as good as MSE: the magnitude of the corresponding SROCC for both  $Q$  and MSE are above 0.9 with low variances. Meanwhile,  $Q$  outperforms JNB [12] since

JNB fails in distinguishing quality decay against high frequency components due to noise. As specific illustrations, plots of MOS versus  $Q$  corresponding to the sample images in Fig. 20(a)–(c) are illustrated in Fig. 20(d)–(f), which show that the metric  $Q$ 's response to blur and noise is very close to the subjective quality perception.

## V. CONCLUSION

In this paper, we proposed an image content metric  $Q$  which can be used in an unsupervised fashion for parameter optimization of any image denoising algorithm. This metric is based upon the singular value decomposition (SVD) of local image gradients. It is properly correlated with the noise level, sharpness and intensity contrast of the structured regions of an image without any prior knowledge. Simulated and real data experiments on denoising filters demonstrated that this metric can capture the trend of quality change during the denoising process, and can yield parameters that show good visual performance in balancing between denoising and detail preservation. Additional tests using blurred and noisy images from the TID2008 database confirm that the proposed metric is well-correlated with subjective evaluations.

It is worth mentioning that because metric  $Q$  only takes structured regions (anisotropic patches) into consideration, the range of its applicability as a general no-reference measure may be limited. For example, it cannot handle situations where noise only appears in flat regions (isotropic patches). However, for the parameter optimization application studied in this paper, implementing  $Q$  using only anisotropic patches is adequate.

Going forward, we envision extending the use of this metric to the parameter optimization problem in other image restoration algorithms, such as deblurring and super-resolution. Research on designing a metric for video content within the same framework is also worth pursuing.

It is also possible to extend  $Q$  as a general no-reference image quality metric. However, it is worth noting that  $Q$  measures image content rather than relative quality. For example, we cannot use  $Q$  directly to compare the quality of a distorted version of *Barbara* with a similarly distorted *Flower* image. A proper normalization would be required to design a metric appropriate for cross-image assessment. This is an interesting direction for further study.

## APPENDIX CALCULATION OF PROBABILITY DENSITY FUNCTIONS

If all components of the gradient matrix  $\mathbf{G}$  are independent standard Normal variables, the joint probability density function for its singular values  $s_1$  and  $s_2$  is given by [25]

$$f_{S_1, S_2}(s_1, s_2) = \frac{1}{(N^2 - 2)!} e^{-\frac{1}{2}(s_1^2 + s_2^2)} s_1^{N^2 - 2} s_2^{N^2 - 2} (s_1^2 - s_2^2). \quad (34)$$

In a more general case, where the variance of a  $N \times N$  white Gaussian noise image is  $\sigma^2$ , its  $\mathbf{G}$  can be viewed as a  $N^2 \times 2$  Gaussian matrix with a variance equals to  $\xi\sigma^2$ , where  $\xi$  is determined by the filters that we choose to calculate the discrete

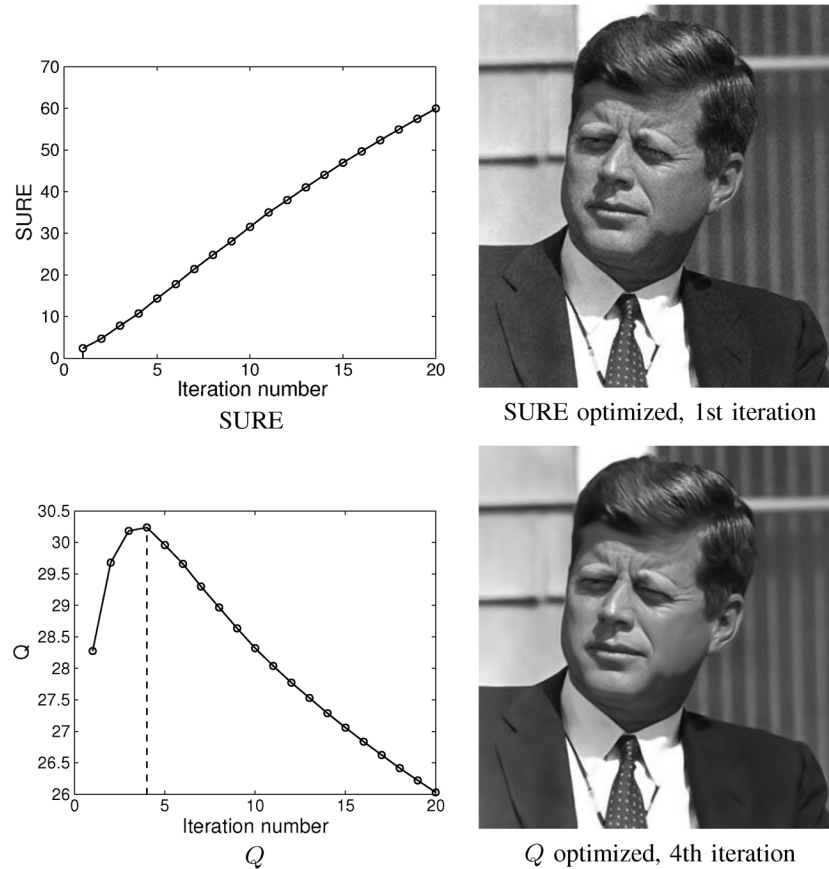


Fig. 18. Plots of SURE and metric  $Q$  versus iteration number in **SKR** denoising experiments using image **JFK**, and optimized filtered images.

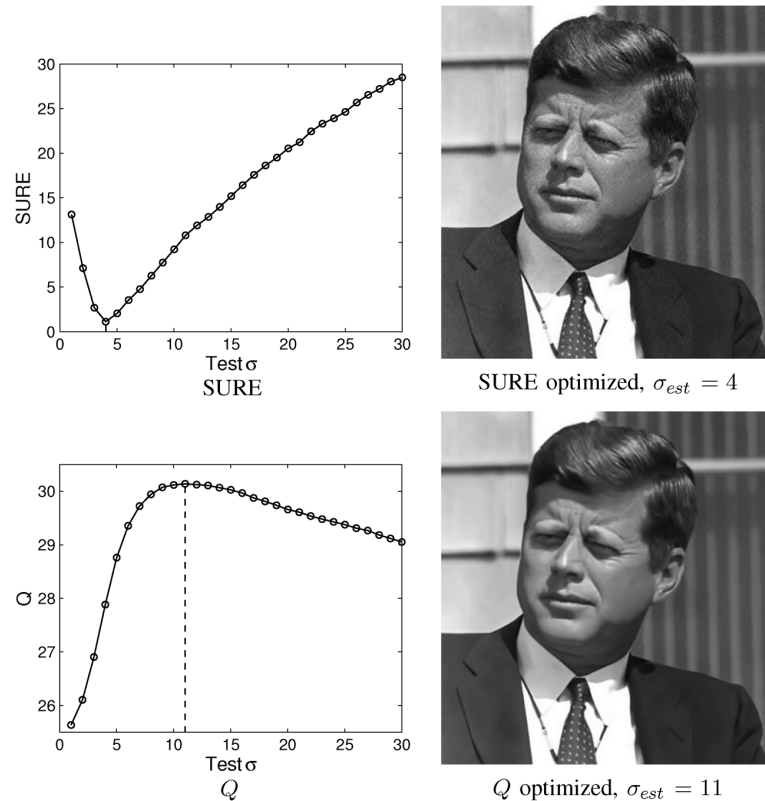


Fig. 19. Plots of SURE and metric  $Q$  versus the tuning parameter in **BM3D** denoising experiments using image **JFK**, and optimized filtered images.

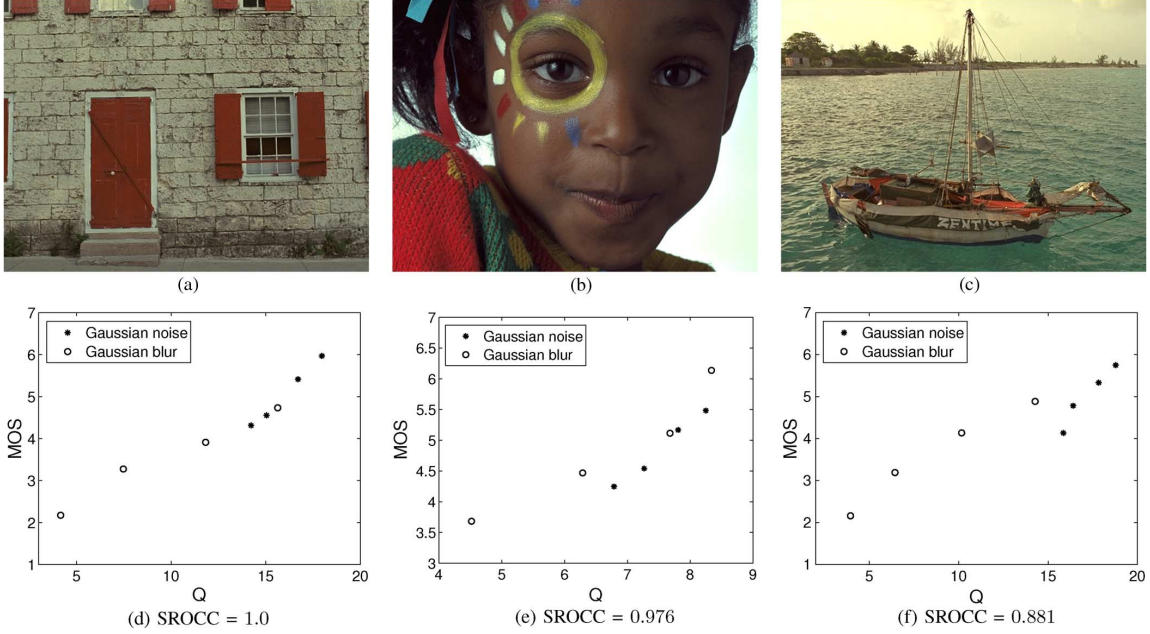


Fig. 20. Sample reference images (a)–(c) from TID2008 database. (d)–(f) Show the plots of MOS versus  $Q$  of the image sets degraded from (a)–(c), respectively, where each set contains images distorted (using Gaussian blur and Gaussian noise) from a single reference.

TABLE I  
MEAN AND STANDARD DEVIATION OF THE SROCC VALUES  
OF FULL-REFERENCE (FR) AND NO-REFERENCE (NR)  
METRICS USING 25 IMAGE SETS FROM TID2008 DATABASE

SROCC	blurry images		noisy images		blur + noise	
	mean	std.	mean	std.	mean	std.
MSE (FR)	-1.0	0.0	-0.992	0.039	<b>-0.930</b>	<b>0.091</b>
Metric $Q$ (NR)	1.0	0.0	0.976	0.086	<b>0.921</b>	<b>0.080</b>
JNB (NR)	1.0	0.0	-0.840	0.339	<b>0.452</b>	<b>0.171</b>

image gradient. The joint density function of the singular values  $s_1$  and  $s_2$  can then be derived from (34) as

$$f_{S_1, S_2}(s_1, s_2) = \frac{\nu^{2N^2}}{(N^2-2)!} e^{-\frac{\nu^2}{2}(s_1^2+s_2^2)} \cdot s_1^{N^2-2} s_2^{N^2-2} (s_1^2 - s_2^2) \quad (35)$$

where  $\nu = 1/(\sigma\xi^{1/2})$ .

The marginal pdf of  $s_1$  is

$$\begin{aligned} f_{S_1}(s_1) &= \int_0^{s_1} f_{S_1, S_2}(s_1, t) dt \\ &= \frac{1}{2(N^2-2)!} e^{-\frac{s_1^2 \nu^2}{2}} s_1^{2\beta-1} \nu^{2\beta} \\ &\cdot \left[ 2(s_1 \nu)^{2\beta} e^{-\frac{s_1^2 \nu^2}{2}} - 2^\beta (2\beta - s_1^2 \nu^2) \gamma\left(\beta, \frac{s_1^2 \nu^2}{2}\right) \right] \end{aligned} \quad (36)$$

where  $\beta = (N^2-1)/2$ , and  $\gamma(a, x)$  stands for lower incomplete gamma function, which is defined as:

$$\gamma(\beta, x) = \int_0^x t^{\beta-1} e^{-t} dt. \quad (37)$$

According to the definition of the sharpness metric  $H$  in (26) and the formula (36), the density function of  $H$  becomes

$$f_H(h) = \frac{1}{2(N^2-2)!} e^{-\frac{h^2}{2\mu^2}} \frac{h^{2\beta-1}}{\mu^{2\beta}} \left[ 2 \left( \frac{h}{\mu} \right)^{2\beta} e^{-\frac{h^2}{2\mu^2}} - 2^\beta \left( 2\beta - \frac{h^2}{\mu^2} \right) \gamma\left(\beta, \frac{h^2}{2\mu^2}\right) \right] \quad (38)$$

where

$$\mu = \frac{\xi^{\frac{1}{2}}}{\sigma + \epsilon/\sigma}. \quad (39)$$

The ratio between  $s_1$  and  $s_2$  is called the condition number  $\kappa$

$$\kappa = \frac{s_1}{s_2} \quad (40)$$

whose pdf is given by [25]

$$f_K(\kappa) = 2^{N^2-1} (N^2-1) \frac{\kappa^2 - 1}{(\kappa^2 + 1)^{N^2}} \kappa^{N^2-2}, \quad 1 \leq \kappa \leq \infty. \quad (41)$$

We note that the coherence  $R$  is related to  $\kappa$  by  $\kappa = (1+R)/(1-R)$ . Using the formula of random variable transformation [26], the pdf of  $R$  can then be derived as

$$f_R(r) = 4(N^2-1)r \frac{(1-r^2)^{N^2-2}}{(1+r^2)^{N^2}}, \quad 0 \leq r \leq 1. \quad (42)$$

Given the joint density function  $f_{S_1, S_2}(s_1, s_2)$  in (35), the conditional density of  $s_2$  given  $s_1$  can be derived as

$$f_{S_2|S_1}(s_2|s_1) = \frac{f_{S_1, S_2}(s_1, s_2)}{f_{S_1}(s_1)}. \quad (43)$$

According to the definition (28), the relationship between  $s_2$  and  $Q$  can also be written as

$$s_2 = s_1 \frac{s_1 - Q}{s_1 + Q}. \quad (44)$$

Again, using the random variable transformation, the conditional density function of  $Q$  given  $s_1$  becomes

$$\begin{aligned} f_{Q|S_1}(q|s_1) &= f_{S_2|S_1}(s_2|s_1) \left| \frac{ds_2}{dq} \right| \\ &= f_{S_2|S_1} \left( s_1 \frac{s_1 - q}{s_1 + q} | s_1 \right) \frac{2s_1^2}{(s_1 + q)^2}. \end{aligned} \quad (45)$$

Then the joint density function of  $s_1$  and  $Q$  can be written as

$$\begin{aligned} f_{Q,S_1}(q, s_1) &= f_{S_1}(s_1) f_{Q|S_1}(q|s_1) \\ &= f_{S_1, S_2} \left( s_1, s_1 \frac{s_1 - q}{s_1 + q} \right) \frac{2s_1^2}{(s_1 + q)^2}. \end{aligned} \quad (46)$$

So the pdf of  $Q$  becomes

$$\begin{aligned} f_Q(q) &= \int_q^\infty f_{Q,S_1}(q, t) dt \\ &= \frac{8q\nu^{2N^2}}{(N^2 - 2)!} \\ &\times \int_q^\infty t^{2N^2+1} \frac{(t - q)^{N^2-2}}{(t + q)^{N^2+2}} e^{-t^2\nu^2 \frac{(t^2 + q^2)}{(t + q)^2}} dt. \end{aligned} \quad (47)$$

#### ACKNOWLEDGMENT

The authors would like to thank the associate editor, Dr. J. E. Folwer, and the anonymous reviewers for their constructive comments and suggestions.

#### REFERENCES

- [1] J. Shen, "Weber's law and weberized TV (total variation) restoration," *Phys. D: Nonlinear Phenom.*, vol. 175, pp. 241–251, 2003.
- [2] Z. Wang, A. C. Bovik, H. R. Sheikh, and E. P. Simoncelli, "Image quality assessment: From error visibility to structural similarity," *IEEE Trans. Image Process.*, vol. 13, no. 4, pp. 600–612, Apr. 2004.
- [3] R. Ferzli and L. J. Karam, "A no-reference objective sharpness metric using Riemannian tensor," in *Proc. 3rd Int. Workshop Video Process. Quality Metrics Consum. Electron.*, Scottsdale, AZ, Jan. 2007, pp. 25–26.
- [4] P. Marziliano, F. Dufaux, S. Winkler, and T. Ebrahimi, "A no-reference perceptual blur metric," in *Proc. Int. Conf. Image Process.*, Rochester, NY, 2002, vol. 3, pp. 57–60.
- [5] G. H. Golub, M. Heath, and G. Wahba, "Generalized cross-validation as a method for choosing a good ridge parameter," *Technometrics*, vol. 21, no. 2, pp. 215–223, May 1979.
- [6] D. A. Girard, "The fast Monte-Carlo cross-validation and  $c_l$  procedures: Comments, new results and application to image recovery problems," *Comput. Statist.*, vol. 10, pp. 205–231, 1995.
- [7] P. C. Hansen, "Analysis of discrete ill-posed problems by means of the L-curve," *SIAM Rev.*, vol. 34, no. 4, pp. 561–580, 1992.
- [8] P. C. Hansen and D. P. O'Leary, "The use of the L-curve in the regularization of discrete ill-posed problems," *SIAM J. Sci. Comput.*, vol. 14, no. 6, pp. 1487–1503, 1993.
- [9] C. Stein, "Estimation of the mean of a multivariate normal distribution," *Ann. Statist.*, vol. 9, pp. 1135–1151, 1981.
- [10] S. Ramani, T. Blu, and M. Unser, "Monte-Carlo SURE: A black-box optimization of regularization parameters for general denoising algorithms," *IEEE Trans. Image Process.*, vol. 17, no. 9, pp. 1540–1554, Sep. 2008.
- [11] Y. Qu, Z. Pu, H. Zhao, and Y. Zhao, "Comparison of different quality assessment functions in autoregulatory illumination intensity algorithms," *Opt. Eng.*, vol. 45, pp. 117–201, 2006.

- [12] R. Ferzli and L. J. Karam, "A no-reference objective image sharpness metric based on the notion of just noticeable blur (JNB)," *IEEE Trans. Image Process.*, vol. 18, no. 4, pp. 717–728, Apr. 2009.
- [13] J. Caviedes and F. Oberti, "A new sharpness metric based on local kurtosis, edge and energy information," *Signal Process. Image Commun.*, vol. 19, pp. 147–161, 2004.
- [14] E. N. Kirsanova and M. G. Sadovsky, "Entropy approach in the analysis of anisotropy of digital images," *Open Syst. Inf. Dynam.*, vol. 9, pp. 239–250, 2002.
- [15] S. Gabarda and G. Cristóbal, "Blind image quality assessment through anisotropy," *J. Opt. Soc. Amer. A*, vol. 24, no. 12, pp. B42–B51, 2007.
- [16] A. Rényi, "Some fundamental questions of information theory," *Selected Papers of Alfréd Rényi*, vol. 3, pp. 526–552, 1976.
- [17] X. Feng and P. Milanfar, "Multiscale principal components analysis for image local orientation estimation," in *Proc. 36th Asilomar Conf. Signals, Syst. Comput.*, Pacific Grove, CA, Nov. 2002, vol. 1, pp. 478–482.
- [18] J. Bigun, G. H. Granlund, and J. Wiklund, "Multidimensional orientation estimation with applications to texture analysis and optical flow," *IEEE Trans. Pattern Anal. Mach. Intell.*, vol. 13, no. 8, pp. 775–790, Aug. 1991.
- [19] X. Zhu and P. Milanfar, "A no-reference sharpness metric sensitive to blur and noise," in *Proc. 1st Int. Workshop Quality Multimedia Experience*, San Diego, CA, Jul. 2009, pp. 64–69.
- [20] H. Takeda, S. Farsiu, and P. Milanfar, "Kernel regression for image processing and reconstruction," *IEEE Trans. Image Process.*, vol. 16, no. 2, pp. 349–366, Feb. 2007.
- [21] K. Dabov, A. Foi, V. Katkovnik, and K. Egiazarian, "Image denoising by sparse 3-D transform-domain collaborative filtering," *IEEE Trans. Image Process.*, vol. 16, no. 8, pp. 2080–2095, Aug. 2007.
- [22] F. R. Hampel, "The influence curve and its role in robust estimation," *J. Amer. Statist. Assoc.*, vol. 69, pp. 383–393, 1974.
- [23] N. Ponomarenko, V. Lukin, A. Zelensky, K. Egiazarian, M. Carli, and F. Battisti, "TID2008—A database for evaluation of full-reference visual quality assessment metrics," *Adv. Modern Radioelectron.*, vol. 10, pp. 30–45, 2009.
- [24] H. R. Sheikh, M. F. Sabir, and A. C. Bovik, "A statistical evaluation of recent full reference image quality assessment algorithms," *IEEE Trans. Image Process.*, vol. 15, no. 11, pp. 3440–3451, Nov. 2006.
- [25] A. Edelman, "Eigenvalues and condition numbers of random matrices," *SIAM J. Matrix Anal. Appl.*, vol. 9, pp. 543–560, 1988.
- [26] P. G. Hoel, S. C. Port, and C. J. Stone, *Introduction to Probability Theory*. Boston, MA: Houghton Mifflin, 1971.



**Xiang Zhu** (S'08) received the B.S. and M.S. degrees in electrical engineering from Nanjing University, Nanjing, China, in 2005 and 2008, respectively, and is currently pursuing the Ph.D. degree in electrical engineering at the University of California, Santa Cruz.

His research interests are in the domain of image processing (denoising, deblurring, super-resolution, and image quality assessment).



**Peyman Milanfar** (F'10) received the B.S. degree in electrical engineering and mathematics from the University of California, Berkeley, and the M.S., E.E., and Ph.D. degrees in electrical engineering from the Massachusetts Institute of Technology, Cambridge, in 1988, 1990, and 1993, respectively.

Until 1999, he was a Senior Research Engineer at SRI International, Menlo Park, CA. He is currently a Professor of Electrical Engineering and associate Dean for research at the University of California, Santa Cruz. He was a Consulting Assistant Professor of computer science at Stanford University, Stanford, CA, from 1998 to 2000, where he was also a Visiting Associate Professor in 2002. His technical interests are in statistical signal and image processing and inverse problems.

Dr. Milanfar won a National Science Foundation CAREER award. He was an Associate Editor for the IEEE TRANSACTION ON IMAGE PROCESSING and was an Associate Editor for the IEEE SIGNAL PROCESSING LETTERS from 1998 to 2001. He is a member of the Signal Processing Society's Image, Video, and Multidimensional Signal Processing (IVMSP) Technical Committee.